ADVANCED MATERIALS
www.advmat.de

Flexible Porous Organic Polymer Membranes for Protonic Field-Effect Transistors

Hong Zhong, Guodong Wu, Zhihua Fu, Haowei Lv, Gang Xu, and Ruihu Wang**

Artificial transistors represent an ideal means for meeting the requirements in interfacing with biological systems. It is pivotal to develop new proton-conductive materials for the transduction between biochemical events and electronic signals. Herein, the first demonstration of a porous organic polymer membrane (POPM) as a proton-conductive material for protonic field-effect transistors is presented. The POPM is readily prepared through a thiourea-formation condensation reaction. Under hydrated conditions and at room temperature, the POPM delivers a proton mobility of 5.7×10^{-3} cm^2 V^{-1} s^{-1}; the charge carrier densities are successfully modulated from 4.3×10^{17} to 14.1×10^{17} cm^{-3} by the gate voltage. This study provides a type of promising modular proton-conductive materials for bioelectronics application.

Proton conduction is a fundamental phenomenon in biological systems.[1,2] A variety of biochemical processes, such as the oxidative phosphorylation in mitochondria,[3] proton pumping in bacteriorhodopsin,[4] and uncoupling membrane potentials by the antibiotic Gramicidin,[5] are associated with ionic and proton transfer. The monitor and control of the proton transfer process by artificial devices represent a desirable approach to interface with biological systems.[6,7] Protonic field-effect transistors (FETs) are a type of promising candidates for bridging between traditional electronics and biological systems. They usually contain three electrodes of source, drain, and gate, in which the proton charge-carrier density in proton-conductive materials could be well modulated by applying different gate bias.[8–12] The conductive materials are known to play pivotal roles in the transduction between biochemical events and electronic signals. Considerable achievements have been made for the synthesis of proton conductive materials from traditional ceramic oxides, solid acids, polymers, and biomaterials to recently reported porous materials, such as metal–organic frameworks and covalent orangic frameworks.[13–16] However, only a few of them have been developed into the channel materials for protonic FETs.[17–19] It is one of the priorities to explore new type of proton-conductive materials and preparation technologies for bioelectronics application of artificial protonic FETs.

Porous organic polymers (POPs) are a type of promising reservoirs for microscopic proton carriers due to their large specific surface area, rich porosity, high stability, and structural modularity.[20–22] POPs could be predesigned with abundant hydrophilic sites to form hydrogen bond networks for facilitating proton hops.[22–24] Taking these structure advantages into account, POPs with high proton carrier mobility and concentration could be fabricated to acquire high protonic conductivity. Most importantly, POPs could be easily processed into membranes with different shapes and sizes through judicial selection of modular building blocks under suitable reaction conditions.[25–28] The mechanical properties of porous organic polymer membrane (POPM) are inherently compatible with those of biological systems, resulting in simple and convenient fabrication for protonic transistor devices. Thus, POPM holds great promises for the transduction of biochemical events and electronic signals. However, to the best of our knowledge, the application of POPM as protonic FETs has not been reported yet.

Thiourea-based polymers possess biocompatible, hydrophilic, low-toxicity, and bioadhesive properties. They have been widely used in biology- and pharmaceutical-related materials.[29,30] Two secondary amine (—NH—) groups in thiourea unit could serve as dual hydrogen bond donors to form strong hydrogen bonds with one oxygen atom in phosphoric acid,[31] which is conducive for the formation of POPs-based gel and membrane. As a proof-of-concept study, herein, we first report a type of thiourea-based POPM as flexible proton-conductive materials. The excellent flexibility and robustness of POPM enable facile fabrication and characterization of POPM-based protonic FETs. The flow of protonic currents could be monitored and controlled with a value as high as 3.3 times by the electrostatic potentials applied to gate electrodes.

Thiourea is one of the promising linkages for the construction of POPs due to its ready formation under mild reaction conditions without any catalysts and byproducts releasing.[28] The thiourea-based POPM was facilely prepared by atom-economic thiourea-formation condensation reaction at ambient temperature. As shown in **Figure 1**a, the *N,N*-dimethylformamide (DMF) solution of 1,3,5-tris(4-aminophenyl)benzene (TAPB) and 1.5 equivalents of 1,4-diisothiocyanatobenzene (DSAB) in the presence of 3.0 equivalents of phosphoric acid

Dr. H. Zhong, Dr. G. Wu, Dr. Z. Fu, H. Lv, Prof. G. Xu, Prof. R. Wang
State Key Laboratory of Structural Chemistry
Fujian Institute of Research on the Structure of Matter
Chinese Academy of Sciences
Fuzhou, Fujian 350002, China
E-mail: gxu@fjirsm.ac.cn; ruihu@fjirsm.ac.cn
Dr. H. Zhong, Prof. G. Xu, Prof. R. Wang
University of Chinese Academy of Sciences
Beijing 100049, China
The ORCID identification number(s) for the author(s) of this article can be found under https://doi.org/10.1002/adma.202000730.

DOI: 10.1002/adma.202000730

 © 2020 WILEY-VCH Verlag GmbH & Co. KGaA, Weinheim

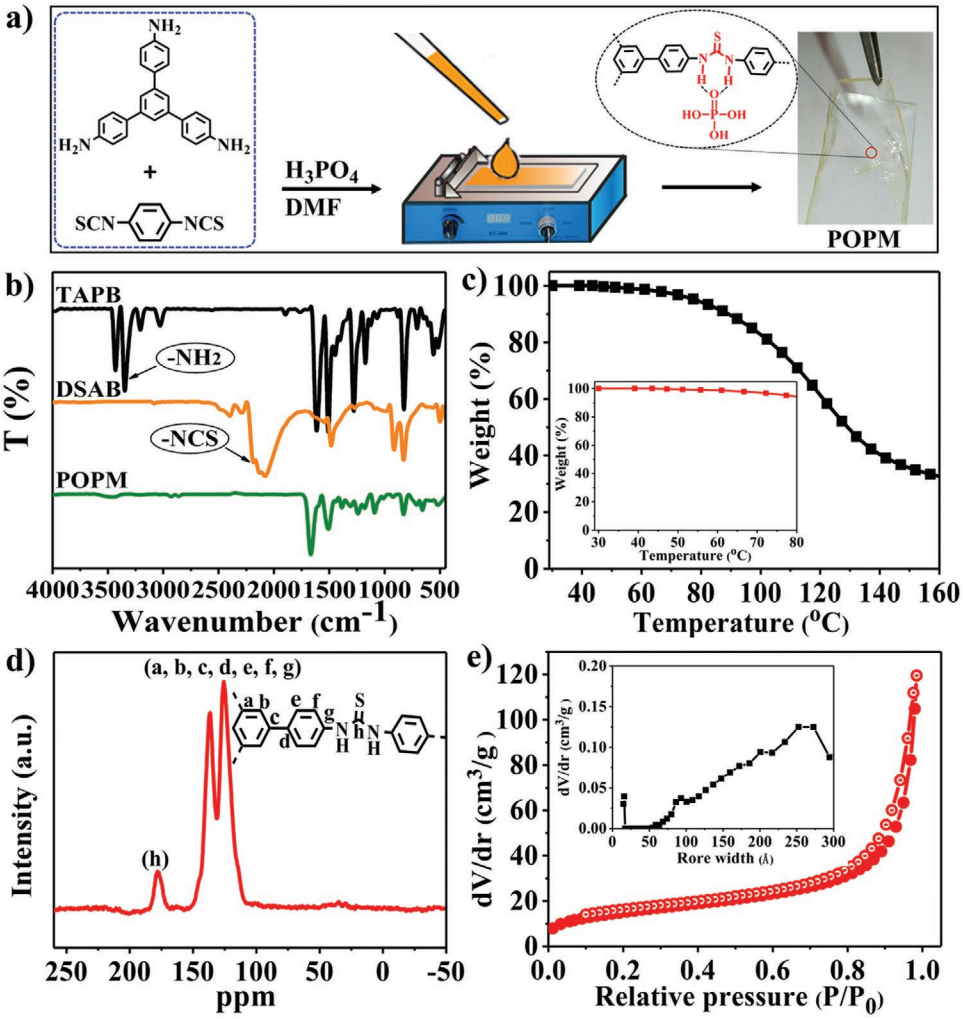

Figure 1. a) Schematic illustration for the prepration of POPM. b) FTIR spectra for TAPB, DSAB, and POPM. c) TGA curves for POPM in different temperature ranges. d) Solid-state ^{13}C NMR spectrum and e) N_2 sorption isotherm of the POPM-xerogel; the inset is pore size distribution.

produced a brown translucent emulsion. After the resultant mixture was painted on a glass substrate and flattened using the other glass sheet, transparent POPM was instantly formed. The thickness of membrane could be modulated through varying amount of starting materials (Figure S1, Supporting Information). Notably, there is no detectable irreversible deformation after POPM is repeatedly folded into high curvature, indicating its good flexibility and mechanical durability (Figure S2, Supporting Information).

The Fourier transform infrared (FTIR) spectra of starting materials and POPM were shown in Figure 1b, both characteristic isothiocyanate stretching band in DSAB at 2074 cm^{-1} and typical N—H peak in TAPB at 3348 cm^{-1} totally disappear, indicating successful coupling of TAPB and DSAB.[28] Thermogravimetric analysis (TGA) measurement exhibits that POPM has no appreciable weight loss until 80 °C (Figure 1c). The first weight loss of 66% occurs at 80–150 °C, which is attributed to the removal of trapped solvent molecules. X-ray diffraction pattern of POPM reveals its amorphous property for the polymer membrane material (Figure S3, Supporting Information). To further characterize the skeletal structure and porosity, a xerogel of the POPM (POPM-xerogel) was prepared through the removal of trapped solvent molecules. In the FTIR spectrum of POPM-xerogel, the peak of the C=O stretching vibration for DMF at 1667 cm disappears, other peaks are the same as that of POPM (Figure S4, Supporting Information). The solid-state ^{13}C NMR spectrum of POPM-xerogel shows a peak at 177 ppm (Figure 1d), which is assigned to the thiourea carbon atom, further confirming the formation of thiourea linkage in POPM. Other peaks in the range of 150–110 ppm correspond to aromatic carbon atoms. No characteristic peak of DMF molecule is observed in the solid-state ^{13}C NMR of POPM-xerogel, which indicates that the trapped solvent molecules were thoroughly removed. The TGA curve of POPM-xerogel indicates that the skeletal structure of POPM is stable before 235 °C (Figure S5, Supporting Information).

The porosity of POPM-xerogel was examined by N_2 physisorption at 77 K (Figure 1e). The N_2 adsorption/desorption provides a type II adsorption branch according to the International Union of Pure and Applied Chemistry classification. The hysteresis at high relative pressure is a clear evidence for the existence of mesopores. The steep rise of N_2 uptake at $P/P_0 > 0.9$ is

© 2020 WILEY-VCH Verlag GmbH & Co. KGaA, Weinheim

probably attributed to the condensation of N_2 molecules in the mesopore and interparticular space. Brunauer–Emmett–Teller-specific surface area, total pore volume, and N_2 uptake amount of POPM-xerogel are 51 m^2 g^{-1}, 0.176 cm^3 g^{-1}, and 121 cm^3 g^{-1}, respectively. These values are comparable with those in reported organic xerogels.[26,28] The pore size distribution indicates that COG-xerogel has a hierarchical pore structure from micropore to macropore. Scanning electron microscopy (SEM) image further reveals the porosity of POPM-xerogel (Figure S6, Supporting Information). These observations have demonstrated that the solvent and guest molecules are entrapped within the internal cavities of POPM, which contribute to increasing the carrier concentration and mobility for achieving high proton conduction.

It is well known that microstructure and morphology of the polymer membranes play important roles in proton exchange and conductivity of protonic transistors.[32,33] To characterize their electrical properties, POPM was fabricated through dropping the mixture of TAPB and DSAB in DMF in the presence of phosphoric acid to the surface of SiO_2/Si wafer with pre-prepared Au or Pd electrodes. The optical pictures indicate that the surface of POPM is relatively smooth and featureless (**Figure 2**a), there are no detectable pinholes on the top surface. Atomic force microscopy (AFM) shows that the membrane has

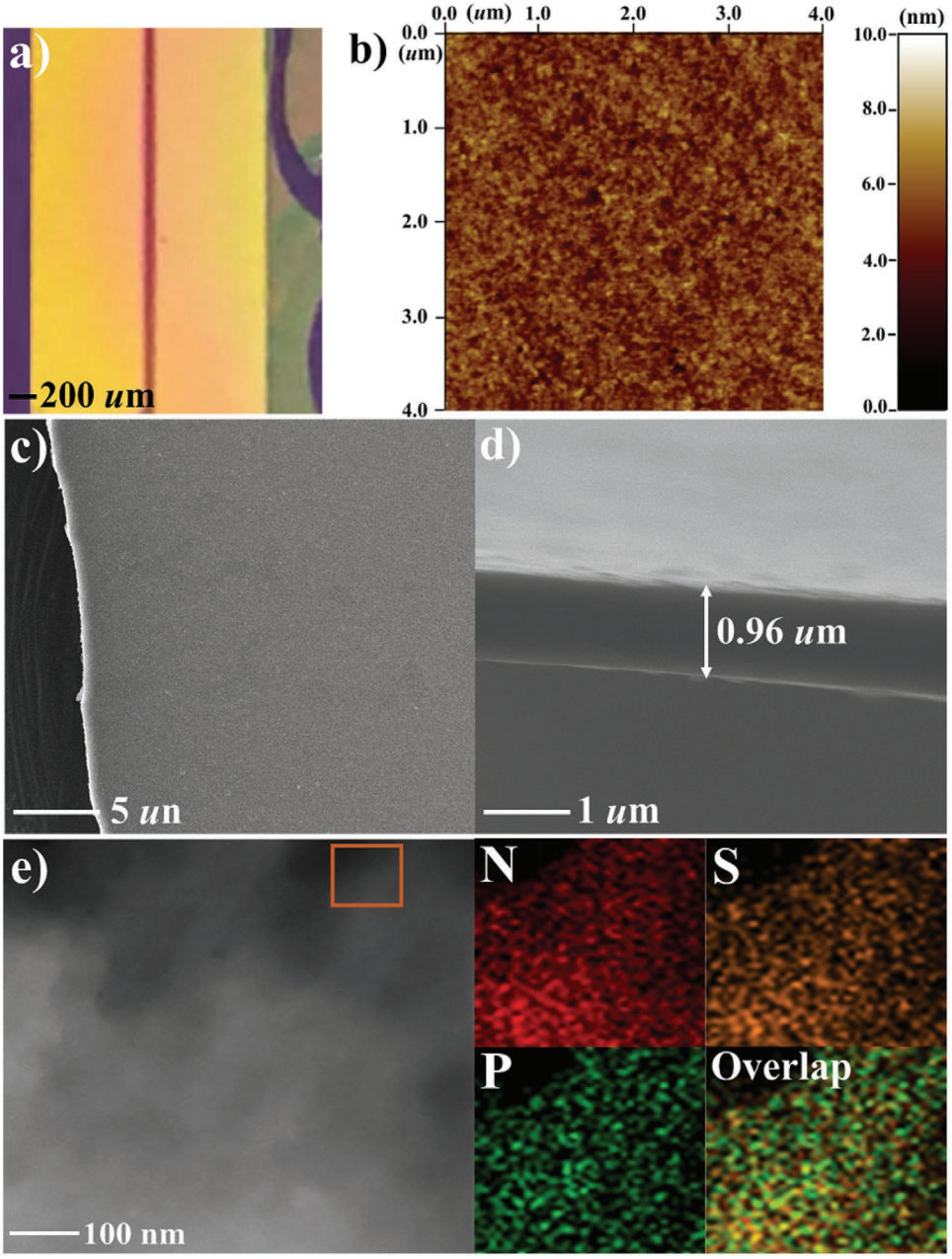

Figure 2. a) Optical image of a device where POPM bridges two electrodes. b) Top-side AFM image of POPM. c) Side and d) cross-sectional SEM images of POPM. e) HAADF-STEM and EDX mapping images of POPM.

© 2020 WILEY-VCH Verlag GmbH & Co. KGaA, Weinheim

a thickness of 0.96 µm (Figure S7, Supporting Information), and the average surface roughness of the top surface is only ≈1.55 nm over an area of 4 µm × 4 µm (Figure 2b). The high quality of top surface shows that solution-prepared technique of POPM is qualified for the fabrication of protonic FET devices.[34] The membrane sandwiched between two electrodes was carefully stripped out for microstructure assessment. SEM images show that POPM exhibits a sheet-like morphology with a smooth topography surface (Figure 2c), and the cross-sectional thickness of the membrane is 0.95–0.98 µm (Figure 2d), which is consistent with the AFM results. High-angle annular dark-field scanning transmission electron microscopy (HAADF-STEM) and energy-dispersive X-ray (EDX) mapping images exhibit that phosphoric acid is uniformly distributed over POPM (Figure 2e), which suggests that POPM could serve as promising candidate of proton reservoirs for proton exchange and conductivity.

The proton conductivity of POPM sandwiched between two Au electrodes was examined by using alternative current electrochemical impedance spectroscopy (EIS) spectra. The relative humidity (RH)-dependent Nyquist plots at 25 °C exhibit that POPM has a proton conductivity of 1.8×10^{-5} S cm^{-1} at 50% RH, which dramatically enhances to 1.1×10^{-3} and 2.8×10^{-3} S cm^{-1} at 90% and 98% RH, respectively (**Figure 3**a,b). The conductivities of POPM are comparable and even superior to those in reported proton-conductive materials.[21,35,36] The increment of proton conductivity with hydration level is mainly attributed that higher level of water adsorption creates more hydrogen-bonded pathways for proton transfer.[36] As comparison, proton conductivity of POPM without phosphoric acid was measured at 25 °C under 98% RH. The conductivity of 5.1×10^{-6} S cm^{-1} is negligible when compared with that of POPM containing 3.0 equivalent of phosphoric acid (Figure S8, Supporting Information), which indicates that protons transfer is predominantly dependent on the oxygen of phosphoric acid. When phosphoric acid loadings are increased from 0.1 to 3.0 equivalents of TAPB, the conductivities gradully enhance, which is attributed that higher ratio of phosphoric acid imparts higher concentration of mobile protons and forms a more extensive hydrogen-bond network for facile proton movement.[26] The proton conductivities of POPM at different temperature were measured in the saturated RH atmosphere and Arrhenius-type conductivity plots were constructed (Figure 3c). The activation energy of proton conduction was estimated to be 0.33 eV by the least-squares fitting in the slopes (Figure 3d), which indicates that proton conductivity in POPM mainly follows the Grotthuss mechanism.[37,38]

Given its good proton conduction properties, POPM was utilized as channel materials to construct protonic FETs. As shown in **Figure 4**a, POPM-based FET with three-terminal configuration was fabricated through sandwiching POPM between palladium electrodes on Si/SiO_2 substrates. The heavily doped Si in Si/SiO_2 wafer was used as the gate electrode. The electronically and protonically conductive palladium hydride (PdH_x) was selected as the source and drain electrodes.[6] The Pd electrodes could be in situ transferred into PdH_x under 5% H_2 atmosphere, which provides continuous supply of protons for the device.

The direct current–voltage (*I*–*V*) curves under different atmosphere conditions were initially measured without applying a gate voltage. The currents under 40% and saturated RH are ≈0.8 and 1.5 nA, respectively (Figure 4b); such small

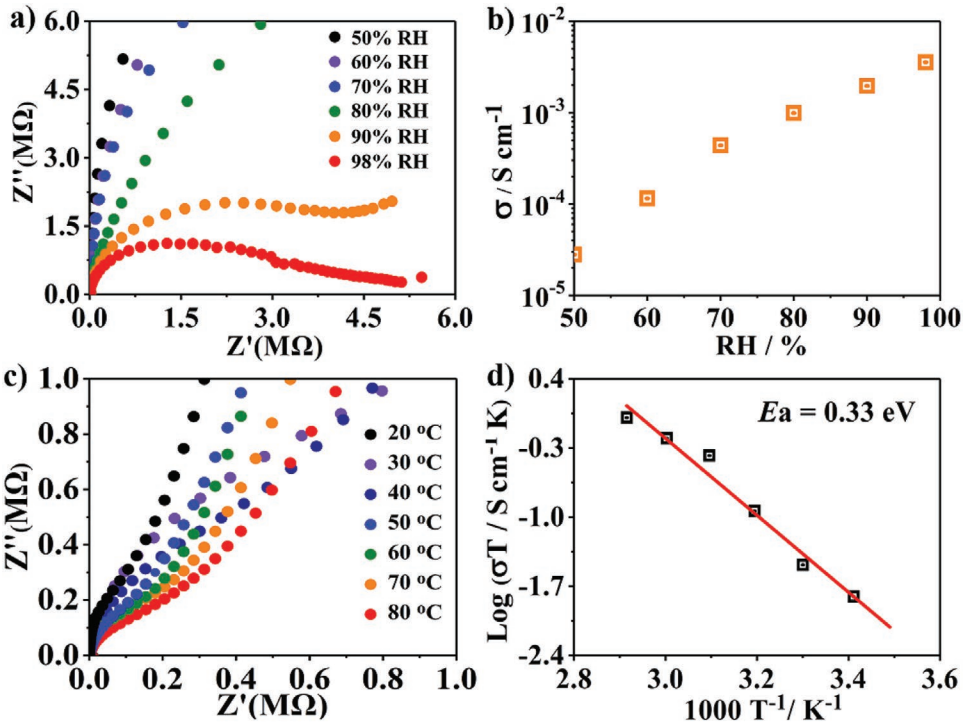

Figure 3. a) RH-dependent Nyquist plots of POPM at 25 °C. b) RH-dependent proton conductivity of POPM. c) Nyquist plots of POPM under different temperatures at 98% RH. d) Temperature-dependent proton conductivity of POPM under 98% RH.

© 2020 WILEY-VCH Verlag GmbH & Co. KGaA, Weinheim

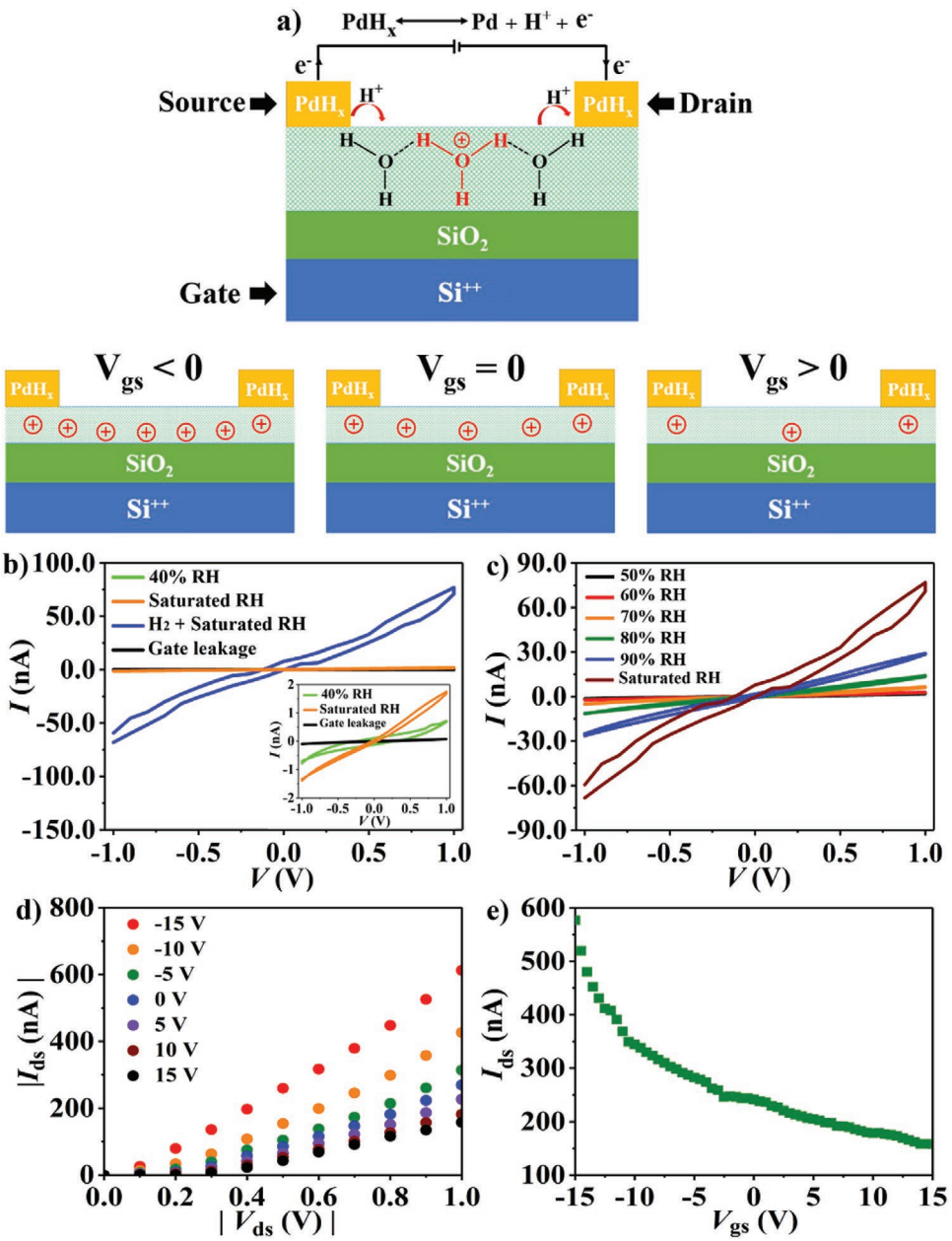

Figure 4. a) Schematic diagram of the configuration of POPM-based three-terminal protonic FETs and its working mechanism. b) *I–V* curves of POPM at different atmosphere conditions. c) *I–V* curves of POPM under 5% H_2 and different RH. d) Typical I_{ds} as a function of V_{ds} at V_{gs} from –15 to 15 V at 5 V steps. e) Plots of the experimental I_{ds} as a function of V_{gs}.

currents reveal the electronically insulating nature of POPM. The similar currents at different RH have corroborated that humidity has little influence on the electronic conduction. However, the current is remarkably enhanced to ≈75 nA under 5% H_2 and saturated RH. The current increment probably originates from in situ formation of proton-conductive PdH_x, which injects more protons into POPM as the charge carriers and enhances protonic current.[6,39,40] In addition, the protonic currents under 5% H_2 show noticeable increase with the rise of RH (Figure 4c), revealing that more water uptake in POPM could induce more hydrogen-bonded pathways and facilitate Grotthuss-type proton conduction.[37] This variation trend agrees well with the aforementioned EIS results. The electrical measurements for these devices give rise to a current density of 5.7×10^{-7} A cm^{-2} at 90% RH at 1.0 V. Moreover, the *I–V* curves display a hysteresis between forward and reverse scans, which is indicative of the ionic nature of charge carriers.[39]

Generally, the *I–V* curves for the electronic currents are similar to each other at different scanning frequencies. However, different *I–V* curves could be observed for protonic currents at varying scanning frequencies because the proton movement has a relaxation effect, while electron transport does not.[41] To further illustrate that the measured currents are indeed protonic currents, the *I–V* testing at different sweep frequencies

 © 2020 WILEY-VCH Verlag GmbH & Co. KGaA, Weinheim

was performed (Figures S9 and S10, Supporting Information). The currents in air have no detectable variation, while the currents under H_2 atmosphere are frequency-dependent. The observations without applying a gate voltage not only have clearly evidenced that the conductivity of POPM is protonic rather than electronic in origin, but also have demonstrated direct detection of proton currents under direct current mode.

The performance of POPM-based protonic FETs was measured under H_2 atmosphere and saturated RH. H_2 concentration has important effects on the device (Figure S11, Supporting Information). The negligible field effect is observed in the absence of H_2. However, by increasing the concentration of H_2 from 1.25% to 2.5% to 5%, proton conductivity is slightly enhanced; thus, 5% H_2 atmosphere is used in the device. As expected for proton-conductive materials on proton-insulating substrate, the gate leakage currents are negligible. The protonic currents between source and drain (I_{ds}) as a function of the voltage between source and drain (V_{ds}) with modulating gate voltage (V_{gs}) are shown in Figure 4d. When a negative V_{gs} is applied, protons are injected into the POPM channel via PdH_x contacts to fulfill the requirement of the capacitor between POPM and gate. The injected protons serve as the additional charge carriers. Thus, higher V_{gs} results in higher I_{ds}. Contrarily, when a positive V_{gs} is applied, protons in the channel are removed due to similar capacitive effect, which results in the decreased I_{ds}. Whatever protons are injected into or excluded from POPM, when one proton crosses contact interface, an electron is detected by the external testing equipment. Therefore, the protonic currents of POPM can be directly monitored by measuring the electronic current with the external equipment. The quasi-linear I_{ds}–V_{ds} curves reveal highly efficient proton-conductive pathways in the POPM channel, and the protons need not overcome an appreciable energy barrier for flowing protonic current. The transfer characteristic of the protonic FET device at $V_{ds} = -1$ V is shown in Figure 4e. The effective proton mobility could be estimated based on the transfer curve in the linear region. The protonic mobility in POPM transistor is calculated to be 5.7×10^{-3} cm^2 V^{-1} s^{-1}, which is comparable with those in reported proton conductors based on dilute acid solutions ($\approx 3 \times 10^{-3}$ cm^2 V^{-1} s^{-1}), maleic chitosan ($\approx 4.9 \times 10^{-3}$ cm^2 V^{-1} s^{-1}), and reflectin (7.3×10^{-3} cm^2 V^{-1} s^{-1}).[17–19]

The proton density in the POPM channel is examined according to the equation $\sigma = e \times n_{H^+} \times \mu_{H^+}$, (where e = proton charge, n_{H^+} = number of free protons per unit volume, and μ_{H^+} = proton mobility).[17,18] Assumed that the proton mobility remains constant at varying gate voltage, the free proton concentration is estimated to be 14.1×10^{17} cm^{-3} at $V_{gs} = -15$ V, 6.6×10^{17} cm^{-3} at $V_{gs} = 0$ V, and 4.3×10^{17} cm^{-3} at $V_{gs} = 15$ V, respectively (Figure S12, Supporting Information). These results have demonstrated that the proton transport in POPM could be effectively modulated by electrostatic voltage.

The stability of POPM-based protonic FETs was also investigated. As shown in Figure S13a, Supporting Information, I_{ds}–V_g curves show that protonic currents degrade obviously with long time intervals for 1–2 weeks, which is attributed that proton devices are sensitive to the external environment. However, these curves almost coincide with each other after repeated tests for 10 times (Figure S13b, Supporting Information), indicative of good short-term stability. It should be mentioned that the repeated tests have an interval of 5 min owing to the relax effect for protons in the protonic FETs. This phenomenon is similar to the effect of short-term memory, which suggests that POPM-based protonic FETs may be used as bionic synaptic devices.

The flexible POPM with high proton mobility has been designed and fabricated. The application of POPM as proton-conductive materials for protonic FETs has been demonstrated for the first time. The efficient proton transfer is performed within the extensive hydrogen-bond network of POPM. POPM-based FET shows the highest proton mobility of 5.7×10^{-3} cm^2 V^{-1} s^{-1} among the reported protonic FETs. Moreover, the protonic current in POPM has been successfully modulated by 3.3 times through gate voltage. Considering unique advantage of POPM in terms of structural modularity and ready functionalization, their physical and electrical properties could be further improved through modulating structure backbones and the incorporated guest molecules. In summary, POPM-based devices have provided exciting research opportunities to protonic FETs for interfacing with living systems.

Experimental Section

Experimental details are provided in the Supporting Information.

Supporting Information

Supporting Information is available from the Wiley Online Library or from the author.

Acknowledgements

H.Z. and G.W. contributed equally to this work. This study was supported by National Key R&D Program of China (2017YFA0206802), National Natural Science Foundation of China (21822109, 21773245, and 21603228), Natural Science Foundation of Fujian Province (2019J01128), and Strategic Priority Research Program of the Chinese Academy of Sciences (XDB20000000).

Conflict of Interest

The authors declare no conflict of interest.

Keywords

field-effect transistors, polymer membranes, porous organic polymers, proton conductivity, protonic transistors

Received: February 1, 2020
Revised: March 6, 2020
Published online: April 17, 2020

[1] T. Genscha, J. Heberle, C. Viappianic, *Photochem. Photobiol. Sci.* **2006**, *5*, 529.
[2] D. R. Weinberg, C. J. Gagliardi, J. F. Hull, C. F. Murphy, C. A. Kent, B. C. Westlake, A. Paul, D. H. Ess, D. G. McCafferty, T. J. Meyer, *Chem. Rev.* **2012**, *112*, 4016.

 © 2020 WILEY-VCH Verlag GmbH & Co. KGaA, Weinheim

[3] E. M. Kuntz, P. Baquero, A. M. Michie, K. Dunn, S. Tardito, T. L. Holyoake, G. V. Helgason, E. Gottlieb, *Nat. Med.* **2017**, *23*, 1234.
[4] S. Wolf, E. Freier, M. Potschies, E. Hofmann, K. Gerwert, *Angew. Chem., Int. Ed.* **2010**, *49*, 6889.
[5] D. Busath, G. Szabo, *Nature* **1981**, *294*, 371.
[6] E. E. Josberger, Y. Deng, W. Sun, R. Kaut, M. Rolandi, *Adv. Mater.* **2014**, *26*, 4986.
[7] Y. Deng, E. Josberger, J. Jin, A. F. Roudsari, B. A. Helms, C. Zhong, M. P. Anantram, M. Rolandi, *Sci. Rep.* **2013**, *3*, 2481.
[8] L. Q. Zhu, C. J. Wan, L. Q. Guo, Y. Shi, Q. Wan, *Nat. Commun.* **2014**, *5*, 3158.
[9] X. Strakosas, J. Selberg, Z. Hemmatian, M. Rolandi, *Adv. Sci.* **2017**, *4*, 1600527.
[10] Z. Hemmatian, T. Miyake, Y. Deng, E. E. Josberger, S. Keene, R. Kautz, C. Zhong, J. Jina, M. Rolandi, *J. Mater. Chem. C* **2015**, *3*, 6407.
[11] D. D. Ordinario, L. Phan, Y. V. Dyke, T. Nguyen, A. G. Smith, M. Nguyen, N. M. Mofid, M. K. Dao, A. A. Gorodetsky, *Chem. Mater.* **2016**, *28*, 3703.
[12] W. K. Lee, J. J. Pietron, D. A. Kidwell, J. T. Robinson, C. L. McGan, P. E. Sheeha, S. P. Mulvaneya, *J. Mater. Chem. C* **2019**, *7*, 10833.
[13] J. C. Liu, Q. Han, L. J. Chen, J. W. Zhao, C. Streb, Y. F. Song, *Angew. Chem., Int. Ed.* **2018**, *57*, 8416.
[14] M. Yoon, K. Suh, S. Natarajan, K. Kim, *Angew. Chem., Int. Ed.* **2013**, *52*, 2688.
[15] E. Fabbri, D. Pergolesi, E. Traversa, *Chem. Soc. Rev.* **2010**, *39*, 4355.
[16] Y. Yoshida, K. Fujie, D. Lim, R. Ikeda, H. Kitagawa, *Angew. Chem., Int. Ed.* **2019**, *58*, 10909.
[17] D. D. Ordinario, L. Phan, W. G. Walkup, J. M. Jocson, E. Karshalev, N. Husken, A. A. Gorodetsky, *Nat. Chem.* **2014**, *6*, 596.
[18] C. Zhong, Y. Deng, A. F. Roudsari, A. Kapetanovic, M. P. Anantram, M. Rolandi, *Nat. Commun.* **2011**, *2*, 476.
[19] R. Fan, S. Huh, R. Yan, J. Arnold, P. D. Yang, *Nat. Mater.* **2008**, *7*, 303.
[20] E. Jeon, S. Y. Moon, J. S. Bae, J. W. Park, *Angew. Chem., Int. Ed.* **2016**, *55*, 1318.
[21] S. Chandra, T. Kundu, S. Kandambeth, R. BabaRao, Y. Marathe, S. M. Kunjir, R. Banerjee, *J. Am. Chem. Soc.* **2014**, *136*, 6570.
[22] Y. Ye, L. Zhang, Q. Peng, G. Wang, Y. Shen, Z. Li, L. Wang, X. Ma, Q. H. Chen, Z. Zhang, S. Xiang, *J. Am. Chem. Soc.* **2015**, *137*, 913.
[23] C. Katsuno, A. Konda, K. Urayama, T. Takigawa, K. Ito, *Adv. Mater.* **2013**, *25*, 4636.
[24] H. Chen, X. Ren, G. Gao, *ACS Appl. Mater. Interfaces* **2019**, *11*, 28336.
[25] O. Kuksenok, P. Dayal, A. Bhattacharya, V. V. Yashin, D. Deb, I. C. Chen, K. J. V. Vliete, A. C. Balazs, *Chem. Soc. Rev.* **2013**, *42*, 7257.
[26] H. Zhong, Z. Fu, J. M. Taylor, G. Xu, R. Wang, *Adv. Funct. Mater.* **2017**, *27*, 1701465.
[27] Y. Wang, M. Lovrak, Q. Liu, C. Maity, V. A. A. le Sage, X. Guo, R. Eelkema, J. H. Esch, *J. Am. Chem. Soc.* **2019**, *141*, 2847.
[28] H. Pan, Z. Cheng, H. Zhong, R. Wang, X. Li, *ACS Appl. Mater. Interfaces* **2019**, *11*, 8032.
[29] N. Pankratova, M. Cuartero, L. A. Jowett, E. N. W. Howe, P. A. Gale, E. Bakker, G. A. Crespo, *Biosens. Bioelectron.* **2018**, *99*, 70.
[30] E. Jaisankar, M. E. Pavithra, S. Krishna, M. Thirumarimurugan, R. S. Azarudeen, *Int. J. Biol. Macromol.* **2020**, *145*, 42.
[31] K. Kumamoto, Y. Misawa, S. Tokita, Y. Kubo, H. Kotsuki, *Tetrahedron Lett.* **2002**, *43*, 1035.
[32] X. Liang, F. Zhang, W. Feng, X. Zou, C. Zhao, H. Na, C. Liu, F. Sun, G. Zhu, *Chem. Sci.* **2013**, *4*, 983.
[33] Y. Guo, Z. Jiang, W. Ying, L. Chen, Y. Liu, X. Wang, Z. J. Jiang, B. Chen, X. Peng, *Adv. Mater.* **2018**, *30*, 1705155.
[34] C. Kataoka-Hamai, Y. Miyahara, *Sci. Technol. Adv. Mater.* **2010**, *11*, 033001.
[35] T. Kobayashi, Y. Li, A. Ono, X. Zeng, T. Ichikawa, *Chem. Sci.* **2019**, *10*, 6245.
[36] D. W. Lim, M. Sadakiyo, H. Kitagawa, *Chem. Sci.* **2019**, *10*, 16.
[37] T. Grancha, J. Ferrando-Soria, J. Cano, P. Amorós, B. Seoane, J. Gascon, M. Bazaga-García, E. R. Losilla, A. Cabeza, D. Armentano, E. Pardo, *Chem. Mater.* **2016**, *28*, 4608.
[38] S. Chand, S. M. Elahi, A. Pal, M. C. Das, *Chem. Eur. J.* **2019**, *25*, 6259.
[39] J. Soto-Rodríguez, Z. Hemmatian, E. E. Josberger, M. Rolandi, F. Baneyx, *Adv. Mater.* **2016**, *28*, 6581.
[40] G. C. Maiti, F. Freund, *J. Chem. Soc., Dalton Trans.* **1981**, *4*, 949.
[41] T. Miyake, M. Rolandi, *J. Phys.: Condens. Matter* **2016**, *28*, 023001.

© 2020 WILEY-VCH Verlag GmbH & Co. KGaA, Weinheim